Nanoscale

Accepted Manuscript

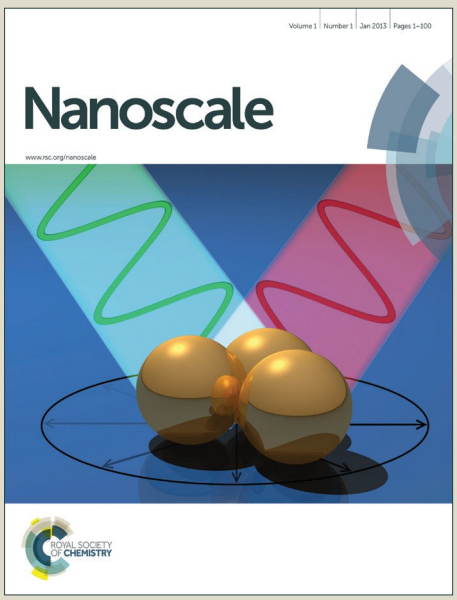

ROYAL SOCIETY OF CHEMISTRY

www.rsc.org/nanoscale

Journal Name

ARTICLE

Quantitative Analysis of the Size Effect of Room Temperature Nanoimprinted P3HT Nanopillar Arrays on Photovoltaic Performance

Received 00th January 20xx,
Accepted 00th January 20xx

DOI: 10.1039/x0xx00000x

www.rsc.org/

Guangzhu Ding,[a, c] Chao Li,[b] Xiaohui Li,[a] Yangjiang Wu,[a] Jieping Liu,[c] Yaowen Li,[b]* Zhijun Hu [a,]*Yongfang Li [b,d]

We develop a solvent-assistant room temperature nanoimprint lithography (SART-NIL) technique to fabricate ideal activ layer consisting of poly(3-hexylthiophene) nanopillar arrays surrounded by [6,6]-phenyl-C61-butyric acid methyl ester. Characterization of scanning electron microscopy, two-dimensional grazing incidence wide angle X-rays diffrac conducting atomic force microscopy reveals that the SART-NIL technique can precisely control the size of P3HT nanopill arrays. With the decrease in diameters of P3HT nanopillar arrays, the P3HT nanopillar arrays exhibit a more preferable face-on molecular orientation, enhanced UV-vis absorption and higher conducting ability along the direction perpendicular to the substrate. The ordered bulk heterojunction film consisting of P3HT nanopillar arrays with diameter of ~45 nm (OBHJ-45) gives face-on orientation, high interfacial areas of 2.87, high conducting ability of ~130 pA and efficient excito diffusion and dissociation. The polymer solar cell (PSC) based on OBHJ-45 film exhibits significantly improved devic performance compared with those of PSCs based on the P3HT nanoapillar arrays with diameters ~100 nm and ~60 nm. We believe that the SART-NIL technique is a powerful tool for fabricating ideal active layer for high performance PS

1. Introduction

Bulk heterojunction (BHJ) polymer solar cells (PSCs)[1] have been the focus of research in the past decade due to some advantages, such as simple preparation under ambient temperature and pressure conditions, light weight, low cost and flexibility.[2-5] The highest power conversion efficiencies (PCEs) of organic solar cells have been increased to 10%.[6-8] Despite significant progress, further increase the PCE to theoretically anticipated level[9] is needed to compete with silicon solar cells and other types thin-film photovoltaic technologies for commercialization. According to the working mechanism of PSCs, the excitons (holes-electron pairs) are dissociated at the interface of donor and acceptor materials, the separated holes and electrons then transport to the anode and cathode through the continuous donor and acceptor phase, respectively, forming the external circuit. Therefore, an ordered bulk heterojunction (OBHJ) morphology consisting of vertically aligned conjugated polymer nanopillar arrays surrounded by the acceptor materials with nanoscale phase separation, moderate crystallized components are particularly important to achieve high performance of PSCs.[10-] Meanwhile, the molecular orientation of organic materials in active layer should also be considered, because the conducting ability is anisotropic along the organic materials backbones or π-π stacking directions.[14-17] However, due to the weak crystallization and complex miscibility of organic materials in blending active layer, it is difficult to obtain well-controlled morphology and microstructure of the blend film quantitatively, which can be used to systematically investigate structure of active layer influence on the performance of PSCs. A slight change in speed or duration of spin cast can even substantially affect the microstructures of heterojunctions and thus the performance of PSCs.[18, 19] Therefore, an effective method of fabricating active layer and constructing a precise picture of the relationship between structure and photovoltaic performance are in urgent need to accelerate the efficiency improvement of PSCs.

Previous report has demonstrated the π-π stacking direction of alternating ester-substituted thieno[3,4-b]-thiophene and benzodithiophene units (PTB) took a vertical (out-of plane) direction in PTB:[6,6]-phenyl-C61-butyric acid methyl ester (PCBM) solar cells.[20] This so-called "face-on" (or "plane-on") molecular orientation enhanced the vertical charge transport

[a] Center for Soft Condensed Matter Physics and Interdisciplinary Research & Collaborative Innovation Center of Suzhou Nano Science and Technology, Soochow University, Suzhou 215123, China email: zhijun.hu@suda.edu.cn;
[b] Laboratory of Advanced Optoelectronic Materials, College of Chemistry, Chemical Engineering and Materials Science, Soochow University, Suzhou 215123, China email: ywli@suda.edu.cn
[c] College of Chemistry and Materials Science, Huaibei Normal University, Huaibei 235000, China
[d] Beijing National Laboratory for Molecular Sciences, Institution of Chemistry, Chinese Academy of Sciences, Beijing 100190, China

† Electronic Supplementary Information (ESI) available: [The one dimensional GIWAXD intensity profiles of diverse type films integrated along the q_z and q_{xy} directions; C-AFM height images, current images and cross-sectional graphes of P3HT thin film with various film thickness; 2D-GIWAXD images of unprocessed P3HT films with various film thickness, and the dark J-V curve of PSCs based on OBHJ-45 film]. See DOI: 10.1039/x0xx00000x

and photovoltaic performance in comparison to that of poly(3-hexylthiophene):PCBM (P3HT:PCBM) devices where an "edge-on" molecular orientation is dominating.[21] This indicates that the face-on molecular orientation is beneficial for the improvement of PSCs. On the other hand, the thermal nanoimprint lithography (NIL) has been proposed as a promising technique not only can be used to fabricate nanopillar arrays due to its high resolution, effective cost and simple process,[22, 23] but also to induce the crystallization and face-on molecular orientation of organic materials due to the effects of self-organization, nanoconfinement, pressure, rheological chain alignment and so on.[16, 24-27] However, the thermal imprinted organic materials are easily oxidized and decomposed at elevated temperatures by the thermal NIL technique,[28, 29] which is potentially detrimental to the performance of PSCs. Furthermore, the unclear size effect of nanopillar arrays on the molecular orientation and photophysical process in active layer limits the further development of thermal NIL technique for the application in high performance PSCs. Recently, we have developed a simple and cost-effective solvent-assistant room-temperature NIL (SART-NIL) technique, making it possible not only to precisely control the size of P3HT nanopillar arrays, but also to induce the face-on molecular orientation of P3HT at room temperature.[30]

In this work, we successfully fabricated ideal OBHJ active layers consisting of vertically aligned P3HT nanopillar arrays with varied diameters and filled PCBM by the SART-NIL method. We systematically investigate the size effect of P3HT nanopillar arrays on the microstructure of active layer and photophysical process of PSCs. A clear relationship between size of P3HT nanopillar arrays, molecular orientation, optical properties, exciton separation and dissociation, electrical conductivity and photovoltaic performance has been established. The PSC based on OBHJ-45 film (with smallest diameter of P3HT nanoapillar arrays, ~45 nm) exhibits the significantly improved photovoltaic performance, especially for the short circuit current density (Jsc) and fill factor (FF).

2. Experimental section

Regioregular conjugated polymer P3HT (M_w 50 000 g mol^{-1}; regioregularity 98%) was purchased from Rieke Metals Inc. and PCBM (purity 99.5%) was obtained from Solenne B. V. Co..

2.1 P3HT nanopillar arrays preparation

Anodic aluminum oxide (AAO) templates were prepared by a two-step anodization method as described on our previous report.[30] In order to obtain flat aluminum sheets, the cleaned aluminum foils were pressed at room temperature under a pressure of 60 bar with a presser. The anodization was performed in 0.3 M oxalic acid solution (40 V or 50 V voltage) or in 0.2 M sulphuric acid solution (20 V voltage) to obtain nanopores with different periods. Finally, the AAO templates were coated with a monolayer of perfluorooctyltrichlorosilane in order to facilitate template separation after nanoimprinting. P3HT was dissolved in chlorobenzene at a concentration of 20 mg mL^{-1} and filtered with 0.25 μm polytetrafluoroethylene filters. P3HT thin films were prepared by spin coating the chlorobenzene solution onto the PEDOT:PSS-coated ITO/glass substrates at a constant speed (1600 rpm) for 10 seconds in ambient air (25°C) and then immediately transferred to a nanoimprinter system (Obducat, Eitre 3) and covered with AAO templates. We note that some solvent remains in the P3HT thin films and thus P3HT is swollen by the remaining solvent. Next, the AAO templates were pressed again the films under pressure (up to 60 bar) at room temperature (25°C) and held for 15 min. During the solvent-assistant room temperature nanoimprinting (SART-NIL) and further solvent evaporation, the morphologies of P3HT thin films are forced by the AAO templates and are not thermodynamically stable. Therefore, after releasing the pressure, vertically aligned P3HT nanopillar arrays were finally obtained.

2.2 Device fabrication

The PSC devices were prepared with P3HT and PCBM as donor and acceptor materials, respectively. First, ITO-coated glass was cleaned with ultrasonication treatment in deionized water, ethanol, acetone and isopropyl alcohol. After drying the glass, PEDOT:PSS (about 30 nm thickness) was spin cast onto the ITO surface treated with ultraviolet ozone. The substrates were then annealed at 125 °C for 20 min in air. P3HT thin films were obtained by spin-coating from chlorobenzene solution onto the PEDOT:PSS-coated ITO/glass substrates for a short time at room temperature (25 °C). The thin films were immediately transferred to a nanoimprinter for the SART-NIL process. After the AAO template was removed from the substrate, vertically aligned P3HT nanopillar arrays were obtained. After that, PCBM in dichloromethane solution (15 mg ml^{-1}) was spin-coated on top of P3HT nanopillar arrays under ambient atmosphere for 60 sec. The rotation speed ranged from 900 to 1400 rpm depending on the feature sizes of P3HT nanopillar arrays. For the contrast devices, planar heterojunction (PHJ) solar cells were also prepared by spin-coating PCBM onto the unprocessed P3HT thin films. The preparation of devices were completed by evaporating a 0.8 nm thickness LiF layer protected by 100 nm aluminum electrode at a base pressure of 4×10^{-4} Pa. The effective photovoltaic area defined by the geometrical overlap between the bottom ITO electrode and the top cathode was 12 mm^2.

2.3 Morphology and Microstructure Characterization

The morphology of samples was characterized with scanning electron microscopy (SEM) (Hitachi S-4800) operating at 15 kV. A thin layer of Au was deposited onto the sample surfaces by sputtering. Two-dimensional grazing incidence wide angle X-ray diffraction (2D-GIWAXD) measurements were carried out at the BL14B1 Beam Line at the Shanghai Synchrotron Radiation Facility in China. The wavelength and the incident angle of the X-ray beam were 0.12398 nm and 0.18°, respectively. A beam stop was put down to block the primary beam during the two dimensional imaging. Data conversion to q space was achieved by calibration using LaB_6 powder. Conducting atomic force microscopy (C-AFM) (MFP-3D-SA, Asylum Research) was used to simultaneously obtain topographical and current images in a contact mode

Platinum/iridium-coated cantilevers (0.2 N m^{-1} spring constant, Nanosensors) were used for the current imaging. The bias voltage applied between the ITO substrate and conducting cantilever (V_{bias}) was 1.2 V for all the measurements. The C-AFM experiments were carried out at atmosphere environments. UV-vis absorption spectra were measured with UV3600 spectrometer (Shimadzu) in transmission mode. Photoluminescence (PL) measurements were conducted with the aid of a HORIBA Fluoromax-4 spectrofluorometer (HORIBA Jobin Yvon) where the excitation wavelength is 450 nm. Current-voltage characteristics of solar cells were investigated under illumination of 100 mW cm^{-2} white light from a Hg-Xe lamp filtered by a Newport 81094 Air Mass Filter, using a Gwinstek SFG-1023 source meter. The external quantum efficiency (EQE) measurements were performed with monochromatic light from Hg-Xe lamp (Newport 67005) in combination with monochromator (Oriel, Cornerstone 260). The response was recorded as the voltage over a 50 Ω resistance, using a lock-in amplifier (Newport 70104 Merlin). A calibrated Si cell was used as reference. All the measurements were performed at ambient atmosphere.

3. Results and discussion

The fabrication procedure of OBHJ PSC based on SART-NIL technique is illustrated in Scheme 1, where P3HT and PCBM were used as donor and acceptor material, respectively. P3HT nanopillar arrays were achieved by pressing porous anodic aluminum oxide (AAO) mold against P3HT thin film at room temperature, which was obtained by spin-coating P3HT chlorobenzene solution onto PEDOT:PSS coated ITO/glass substrate. Subsequently, PCBM was spin-coated onto the surfaces of P3HT nanopillar arrays under ambient atmosphere. LiF and electrode were finally deposited onto the PCBM surface, successively, to complete the fabrication of OBHJ PSCs. In order to obtain a well-defined and stable active layer with bicontinuous pathways, fabrication of highly reproducible and well-controlled P3HT nanopillar arrays is very important. Here, we successfully obtain the nanoimprinted OBHJ active layer with well-defined P3HT nanopillar arrays by taking advantage of the residual solvent remained in the P3HT thin film after a short time spin-coating, which lower the rigidity of the polymers during the NIL process.[28] To facilitate template separation after imprinting, the AAO mold was also treated with fluorinated silane in gas phase to obtain lower energy surface.[31] Moreover, dichloromethane was chosen as a solvent of PCBM due to much better solubility for PCBM than P3HT, allowing us successfully depositing PCBM layer without destroying the underlying P3HT nanopillar arrays. Finally, OBHJ films bearing P3HT nanopillar arrays with varied diameters of ~100 nm (named OBHJ-100), ~60 nm (OBHJ-60) and ~45 nm (OBHJ-45) were successfully fabricated by changing the sizes of AAO molds.

3.1 Morphology and Microstructure of P3HT nanopillar arrays

Fig.1 shows the top-down SEM images of P3HT films bearing nanopillar arrays, and PCBM films deposited on the surface of

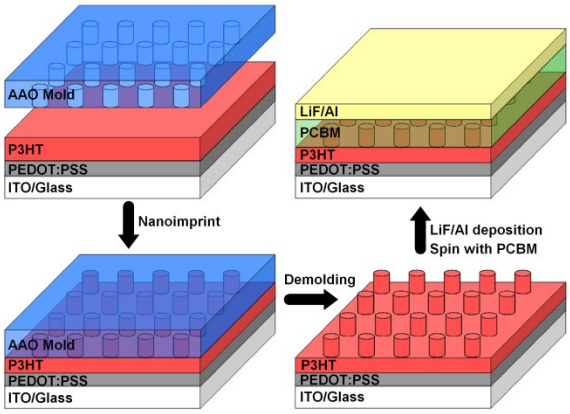

Scheme 1. Procedure for the fabrication of OBHJ PSCs by SART-NIL technique.

P3HT nanopillar arrays, respectively. The P3HT thin films shown in Fig.1a-c contain well-defined and regular hexagonal packed nanopillar arrays with the varied diameters of ~45 nm, ~60 nm and ~100 nm, which are uniformly dispersed throughout the films. To gain a good contact between donor and acceptor materials accompanying a higher coverage of PCBM, we carefully controlled the deposition conditions of PCBM such as the selection of solvent, solution concentration and spin-coating speed. As shown in Fig. 1d, the P3HT nanopillar arrays with a diameter of ~ 60 nm are fully covered by PCBM and the thin film surface shows no obvious defect. We note that some fissures may be observed in the SEM images, which arise from the metal (Au) deposited onto the surfaces.

In our previous study, we have demonstrated that the SART-NIL method can be used not only to fabricate P3HT nanopillar arrays with varied diameters, but also to induce preferential molecular orientation in P3HT nanopillar arrays[30] at room temperature. In order to reveal the molecular orientation in

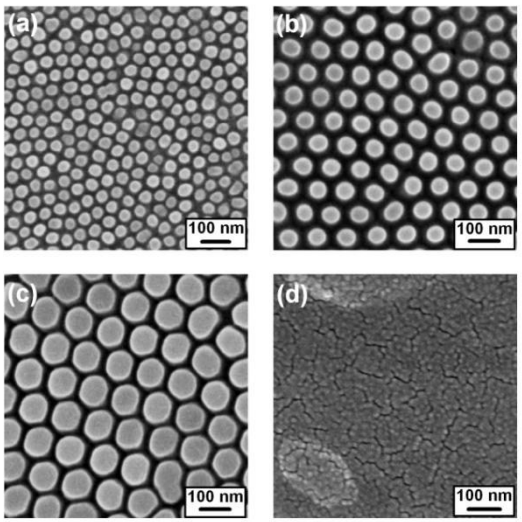

Fig.1. Top-down SEM images of P3HT nanopillar arrays with varied diameters of (a) ~45 nm, (b) ~60 nm, and (c) ~100 nm. (d) Top-down SEM image of PCBM surface deposited on the surface of P3HT nanopillar arrays with a diameter of ~60 nm.

Journal Name

ARTICLE

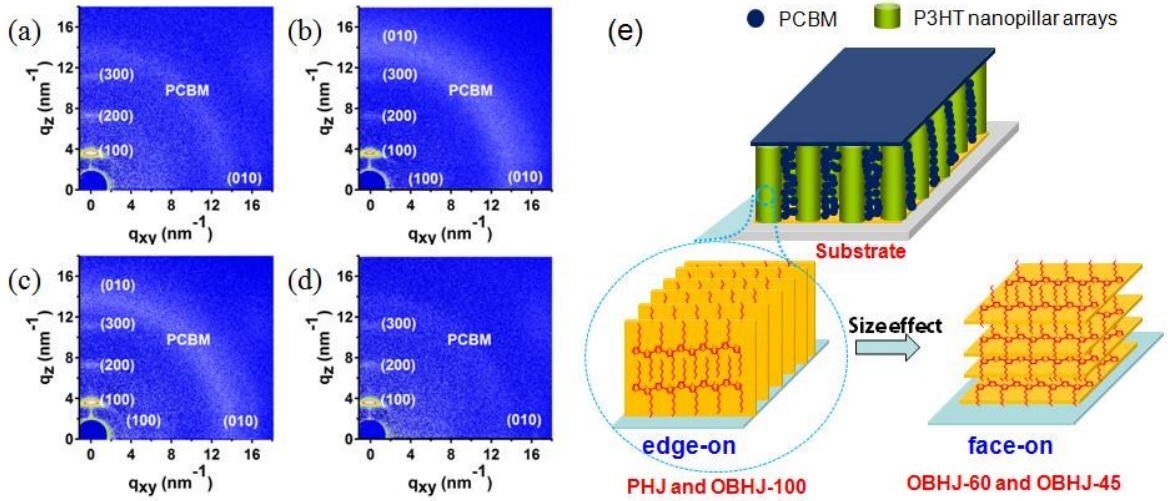

Fig. 2. 2D-GIWAXD images of heterojunction films: (a) PHJ with thickness of 100 nm; OBHJ bearing P3HT nanopillar arrays with the varied diameters of 45 nm (b), 6[illegible] nm (c) and 100 nm (d). (e) Schematics of OBHJ film structure and size effect on the molecular orientation of P3HT nanopillar arrays.

P3HT nanopillar arrays after deposition of PCBM (OBHJ) and the size effect of P3HT nanopillar arrays on the molecular orientation, 2D-GIWAXD experiments were performed and the corresponding images are presented in Fig. 2b-d. Meanwhile, a planar heterojunction-bilayer (PHJ), which was fabricated by spin-coating PCBM solution on the surface of an unprocessed P3HT thin film under the same conditions, was also shown in Fig. 2a for comparison. The one dimensional integrated intensity profiles extracted from the 2D-GIWAXD images along the q_z and q_{xy} directions were also shown in Fig. S1 (Supporting Information). We define here the diffraction vector q_{xy} and q_z pointing along and normal to the substrate plane. As shown in Fig. 2a and d, both the PHJ film and OBHJ film bearing P3HT nanopillar arrays of 100 nm diameter exhibit the (*h*00) and (010) reflections in the q_z and q_{xy}, respectively, indicating that edge-on molecular orientation of P3HT dominates these thin films. Moreover, the 2D-GIWAXD images of unprocessed P3HT films with varied thicknesses (120, 50 and 20 nm) exhibit similar reflections with that of above PHJ film with thickness of 100 nm (Fig. S2). This indicates that the unprocessed P3HT films without external-treatment like SART-NIL method, are dominated by the edge-on molecular orientation of P3HT, which is independent of film thickness. In contrast, the OBHJ films with P3HT nanopillar arrays of ~45 nm (OBHJ-45) and ~60 nm (OBHJ-60) in diameters (Fig. 2b and c) display additional reflections of (010) plane and (100) plane along the q_z direction and q_{xy} direction, respectively. These results confirm that the face-on molecular orientation is prevalent in the P3HT nanopillar arrays with smaller diameters (45 nm and 60 nm), which are consistent with our previous report.[30] Meanwhile, the process of PCBM depositing on the P3HT nanopillar arrays do not affect the P3HT molecular orientation as well. Th[illegible] preferential face-on molecular orientation in OBHJ-45 a[illegible] OBHJ-60 films changing from the edge-on molecula[illegible] orientation in OBHJ-100 film is mainly resulted from the mor[illegible] confinement of rod-like crystals with the decrease in diameter of P3HT nanopillar arrays giving their π-π stacking directio[illegible] along the rod axis. As shown in Fig. 2e, the size effect of P3HT nanopillar arrays on the molecular orientation can be observe[illegible] more clearly. Notably, the diffractions arising from PCBM material are also observed at q=13.8 nm^{-1} in the OBHJ and PH[illegible] films,[32, 33] indicating again that the acceptor material PCBM is indeed deposited on the surface of P3HT nanopillar arrays.

3.2 Optical Properties of OBHJ

To further investigate the influence of P3HT nanopilla[illegible] arrays fabricated by the SART-NIL technique on the optica[illegible] absorption, UV-vis absorption spectra (Fig. 3a) of OBHJ fi[illegible] with varied diameters of P3HT nanopillar arrays and PHJ film with the same thickness for comparison were measured. A[illegible] the absorption spectra show peaks at around 335 nm (typica[illegible] absorption of PCBM), 517 nm and 552 nm (P3HT π-π transitions), and a clear vibronic shoulder at near 600 nm (P3HT inter-chain π-π interaction). The peaks of P3HT a[illegible] around 517 nm, 552 nm and 600 nm are the typical absorptio[illegible] peaks of the crystallized P3HT,[33-35] indicating that P3H[illegible] exhibits ordered arrangement to a certain extent. In addition the absorption intensity of P3HT is generally enhanced afte[illegible] the SART-NIL process. It is particularly noteworthy that the absorption intensity of P3HT nanopillar arrays in OBHJ films [illegible] gradually increased with the decrease in diameters of P3HT nanopillar arrays. As the amount of materials is not changed

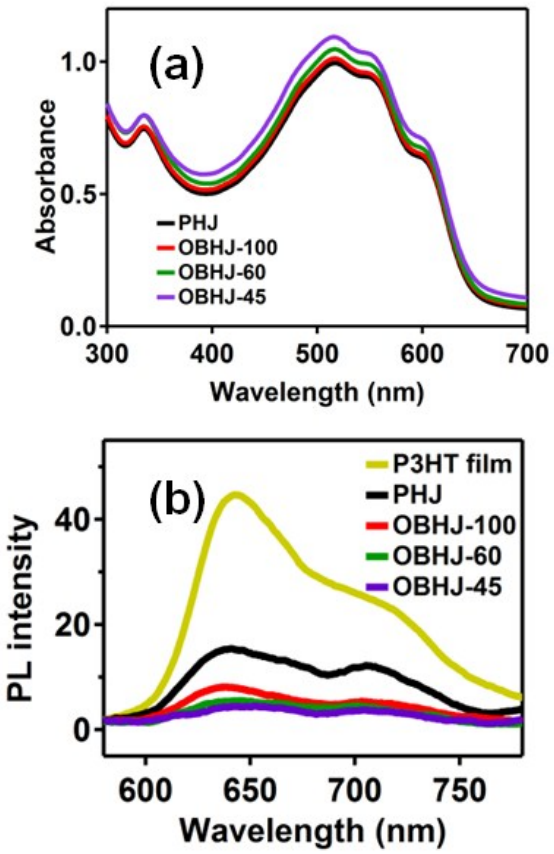

Fig. 3. Unprocessed P3HT film, PHJ film and OBHJ films with varied diameters of P3HT nanopillar arrays (45 nm, 60 nm and 100 nm): (a) UV-vis absorption spectra; (b) PL spectra.

after the SART-NIL process, the enhancement of UV-vis absorption intensity can be attributed to several effects such as light trapping and preferential face-on molecular orientation. The periodic structures can enhance light trapping and thereby increase the absorption by increasing the optical pass length.[36-39] The preferential face-on molecular orientation of crystallized P3HT may also contribute to the enhancement of UV-vis absorption.[40] The higher degree of face-on orientation accompanying the enhancement of UV-vis absorption intensity can be quantitatively confirmed by the ratio of P3HT diffraction intensity at (010) position to (300) location in the q_z direction of the 2D-GIWAXD measurements. The increased diffraction intensity ratios from 0.35 to 0.70 for OBHJ-60 and OBHJ-45 films (as shown in Fig. S1 of Supporting Information), respectively, confirms the higher degree of face-on molecular orientation in OBHJ-45 film, which can enhance the UV-vis absorption intensity of OBHJ film due to the vertical angle between plane of face-on molecules and the incident sunlight.

Photoluminescence (PL) spectra of unprocessed P3HT film, PHJ film and OBHJ films with varied diameters of nanopillar arrays are measured and compared in Fig. 3b, which are used to investigate the size effect of P3HT nanopillar arrays on the exciton diffusion and dissociation. The unprocessed P3HT film exhibit a strong emission peak in the range of 600-750 nm, suggesting a radiative decay pathway. After spin-coating PCBM on the unprocessed P3HT film composing PBHJ film, the emission intensity is obviously decreased to ca. 15%. The incomplete emission quenching indicates both the radiati and nonradiative decay pathways existing in the PBHJ film, as result of the insufficient charge transfer (CT) occurs betwee P3HT and PCBM interface originated from the smalle interfacial area of planar interface. Furthermore, the OBH films give continuously descending emission intensity with the decrease in diameters of P3HT nanopillar arrays. For the OBH 45 film, both the visible emission and the band-edge emission are almost completely quenched. Such a dramatic quenchin in PL emission indicates a prevalent nonradiative decay pathway, owing to the larger interfacial area and smaller spacing between nanopillar arrays (less than 15 nm) giving a nanoscale phase separation, which are beneficial for th exciton dissociation rate and exciton diffusion due to th limited exciton diffusion length of polymers (< 15 nm).[41, 42]

3.3 Conducting ability of OBHJ

In order to investigate the size effect of P3HT nanopillar arrays on the conducting ability. C-AFM was used investigate the in situ conducting ability of P3HT film in the vertical direction. Fig. 4 shows the typical C-AFM heig... current images and corresponding cross-sectional curre graphs of P3HT nanopillar arrays with varied diameters and unprocessed P3HT film for comparison. A flat film an hexagonal P3HT nanopillar arrays with varied diameters can b clearly observed from the unprocessed P3HT film and imprinted nanopillar arrays films (Fig. 4 a1-d1), respectivel which are identical to the SEM images in Fig. 1. As shown in Fig. 4 a2, by applying 1.2 V bias between the conductive substrat and cantilever, a mean current of 25 pA, which uniformly distributed over the entire thin film, was observed in th unprocessed P3HT thin films (~ 50 nm thickness). Moreover, the unprocessed P3HT films with different thicknesses (fro ~20 nm to ~120 nm) give a close current around 25 pA (Fig. S3), which indicates that the conducting ability is independent thickness. The similar conducting ability in the unprocessed P3HT films with varied thicknesses is mainly determined by their unanimous edge-on molecular orientation. Thi conclusion can be further confirmed by the edge-on molecula orientation dominating P3HT nanopillar arrays with diame of ~100 nm, which also exhibits similar conducting abilit (current of ca. 25 pA, Fig. 4 b3) with those of unprocesse P3HT films. Furthermore, the P3HT nanopillar arrays wit diameter of ~60 nm gives a current of ca. 70 pA, about 2 time higher than that of the unprocessed film. The significantl improved conducting ability could be attributed to it preferential face-on molecular orientation, which allows π-π stacking orientation perpendicular to the substrate. Due to th favorable electron delocalization along the π-π stacking direction compared to the side chain direction, the face-o orientation of P3HT molecules is desirable for charge transportation along the direction perpendicular to th substrate, leading to an enhancement in conducting ability. Importantly, this superior conducting ability is desired for the charge carrier transportation in BHJ PSCs. By further

Journal Name

ARTICLE

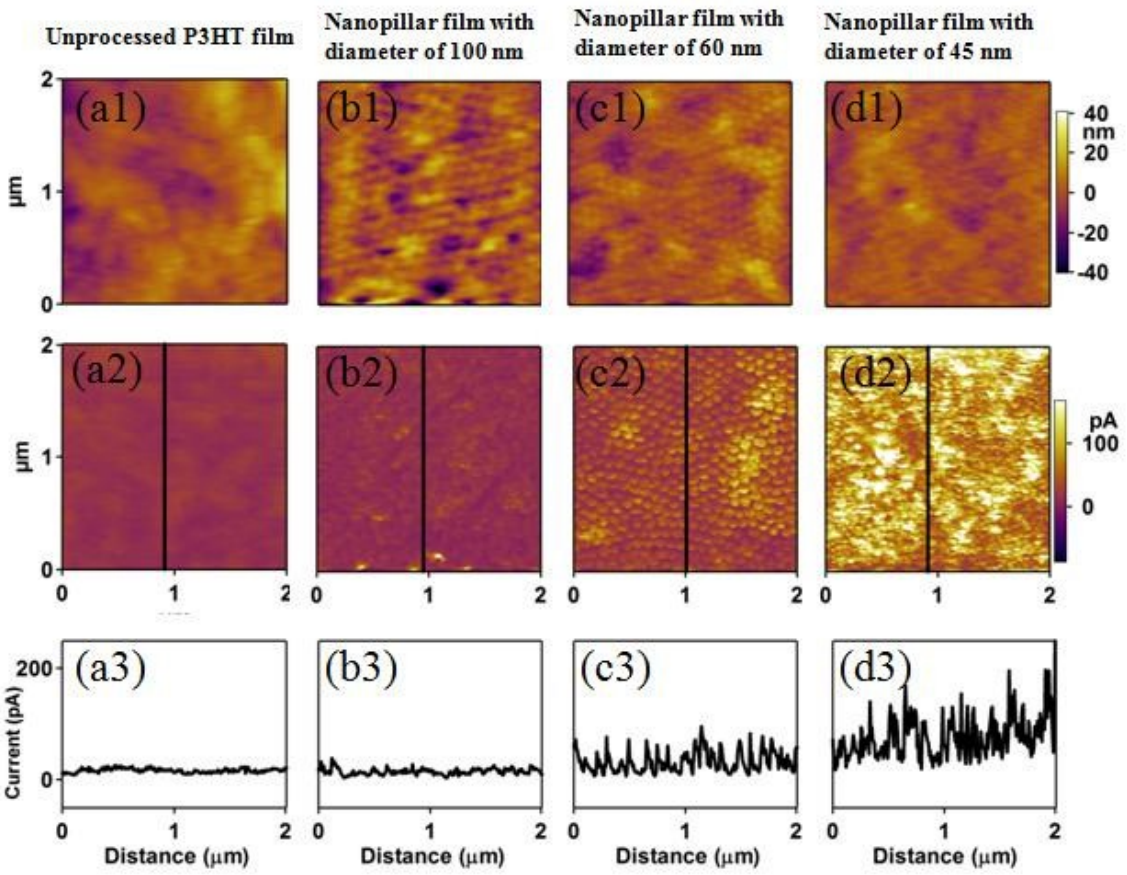

Fig. 4. C-AFM height images, current images and cross-sectional current graphs of an unprocessed P3HT film (a) and P3HT films bearing nanopillar arrays with diameter of 100 nm (b), 60 nm (c) and 45 nm (d). The column from up to down are the height images (alphabet 1), current images (alphabet 2) and cross-sectional current profiles (alphabet 3), respectively.

decreasing the diameter of P3HT nanopillar arrays to ~45 nm, the average current (~130 pA) flowing through the P3HT nanopillar arrays is raised about 2 times higher than that of P3HT nanopillar arrays with diameter of ~60 nm. Because the P3HT nanopillar arrays with smaller diameters are dominated by a higher face-on orientation ratio. Therefore, it further confirms that the face-on molecular orientation is able to enhance the charge transportation along the direction perpendicular to the substrate.

3.4 Photovoltaic cells

We studied how these OBHJ film bearing P3HT nanopillar arrays with varied diameters (OBHJ-100, OBHJ-60 and OBHJ-45), which were fabricated by SART-NIL technique, impact the performance of photovoltaic devices. The photovoltaic properties of active layers based on OBHJ and PHJ for comparison were evaluated by fabricating PSCs with a conventional device structure (ITO/PEDOT:PSS/PHJ or OBHJ/LiF/Al). Fig. 5a and b show the current density-voltage (*J-V*) curves and EQE curves of the PSCs, respectively. The corresponding parameters are given in Table 1. All the measurements were performed under ambient atmosphere and at room temperature. All the devices show a similar open circuit voltage (V_{oc}, 0.50-0.51 V) values, which are approaching those of BHJ PSCs based on P3HT:PCBM blend film (0.55 V),[3] confirming that current generation from exciton dissociation at the interfaces between P3HT nanopillar arrays and PCBM occurs in all of the devices.[43] The slightly lower V_{oc}s are attributed to the relatively higher leakage current (Figure S4) which may be caused by the imperfect OBHJ film due to the slight solubility of dichloromethane in P3HT nanopillar arrays when spin-coating dichloromethane solution of PCBM. In contrast to the similar V_{oc} values, the PSCs based on OBHJ film show significantly improved J_{sc} (from 3.80 to 6.94 mA/cm^2) due to the formation of bicontinuous transportation pathways

Table 1. Characteristic Photovoltaic Parameters from Device under the Illumination of AM 1.5G, 100 mW/cm2.

Active layer	A/A_0 [a]	V_{OC} [V]	J_{SC} [mA/cm^2]	FF	PCE (%)
PHJ	1.00	0.50	3.80	0.46	0.88
OBHJ-100	2.42	0.50	4.80	0.46	1.08
OBHJ-60	2.71	0.51	5.95	0.54	1.66
OBHJ-45	2.87	0.51	6.94	0.59	2.11

[a] A/A_0 is the calculated interfacial area ratio of active layer in OBHJ PSCs.

(P3HT nanopillar arrays and filled PCBM) by SART-NIL technique. One reason for the improved J_{sc} is attributed to the enhanced absorption intensity of P3HT nanopillar arrays based OBHJ films, which can absorb more photons from sunlight. Another reason for the significantly improved J_{sc} is attributed to the vertically aligned P3HT nanopillar arrays in OBHJ film, which can effectively raise the interfacial area. The OBHJ-100 based active layer shows 2.42 times interfacial area than that of PHJ based active layer, which can efficiently increase the exciton dissociation efficiency, therefore leading to the improvement of J_{sc}. It is noteworthy that although the interfacial area of the OBHJ-45 based active layers is only 18% higher than that of OBHJ-100, the PSC based on OBHJ-45 exhibits 45% improved J_{sc} (6.94 mA/cm^2). This indicates that the J_{sc} of PSCs based on OBHJ film are not only determined by the interfacial area, but also by some other factors.

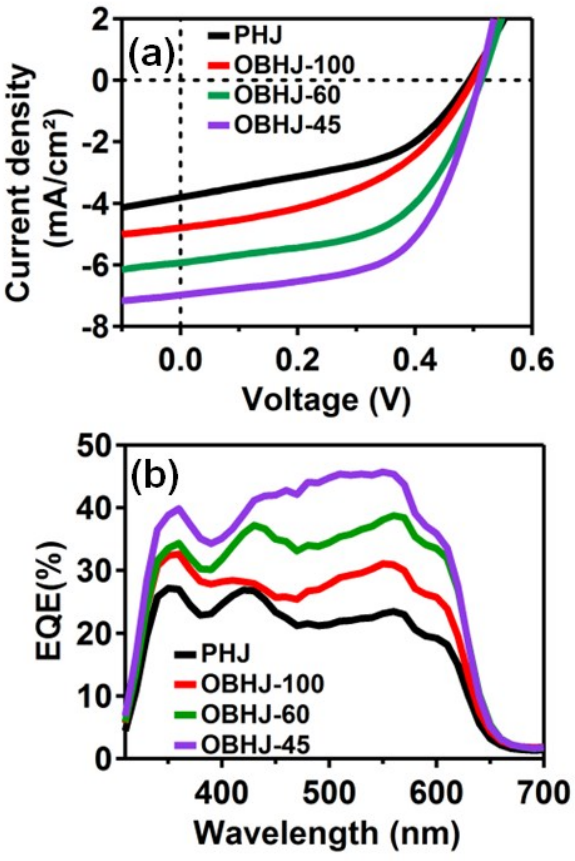

Fig. 5. PSCs based on PHJ film and OBHJ film: (a) J-V curves and (b) EQE curves.

Considering about the mechanism of bulk heterojunction PSCs, the shorter pathway of exciton diffusion and high efficiency of exciton transportation can facilitate the photocurrent generation. With the decrease in diameters of P3HT nanopillar arrays, the excitons can more easily reach the interface between P3HT and PCBM due to the decrease in spacing of nanopillar arrays, which can shorten the pathway of exicton diffusion and then raise the amount of dissociated excitons. Therefore, the decrease in diameter of P3HT nanopillar arrays contributes to the improvement of J_{sc} in certain extent, especially for PSCs based on the smaller diameters of P3HT nanopillar arrays (OBHJ-60 and OBHJ-45). Meanwhile, the alteration of molecular orientation from edge-on to face-on giving an improved conducting ability favors for reducing exciton recombination rate, which can facilitate the further improvement of J_{sc} for the PSCs based on OBHJ-60 and OBHJ-45.

In the case of FF, with the decrease in diameters of P3HT nanopillar arrays, the FFs were gradually improved from 0.46 to 0.59. The increased FFs are mainly attributed to the enhanced conducting ability (hole mobility of P3HT nanopillar arrays), which is dependent on the prevalent face-on orientation, and hence reduce the exciton recombination rate. Furthermore, the improved exciton dissociation efficiency resulting from the increased interfacial areas can also help to reduce the exciton recombination rate during their dissociation process. Notably, the PSCs based on OBHJ-45 showed the highest FF (0.59), indicating the lowest recombination losses, owing to the more prevalent face-on molecular orientation and high interfacial areas in OBHJ-45 film. Overall, these results firmly confirm that SART-NIL technique is an effective method to fabricate the ideal active layer bearing bicontinuous transportation pathways and prevalent face-on molecular orientation by precisely controlling the size of nanopillar arrays, which can provide the large interfacial areas, high conducting ability, efficient exciton diffusion and dissociation, leading to the significant improvement of photovoltaic performance.

The EQE curves of PSCs based on PHJ and OBHJ are shown in Fig. 5b. The EQE curves exhibit a broad response covering 300 - 700 nm wavelength and the calculated J_{sc} values from the integrals of EQE curves are consistent with J_{sc} of J–V measurement. The EQE spectra show the similar shape with their corresponding absorption spectra, indicating that both components (P3HT and PCBM) contribute to the photocurrent. Furthermore, the OBHJ films with varied diameters of P3HT nanopillar arrays also influence the photocurrent contribution. The PSC based on OBHJ-45 with smaller diameter shows larger EQE value and broader response region, especially in the visible region, owing to the more efficient exciton transportation and dissociation.

4. Conclusion

In summary, PSCs based on bicontinous nanopillar arrays consisting of P3HT as donor and PCBM as acceptor were fabricated by the simple and cost-efficient SART-NIL technique. The SART-NIL process was able to not only transfer topographical nanostructure from the template to a P3HT thin film but also precisely control the size of nanopillar arrays at room temperature. We have systematically investigated the relationship between size of P3HT nanopillar arrays and molecular orientation in the P3HT nanopillar arrays. With the decrease of diameter of P3HT nanopillar arrays, the molecular orientation can be changed from edge-on to face on, which can enhance UV-vis absorption and conducting ability along the direction perpendicular to the substrate. Combining the size effect of P3HT nanopillar arrays and preferable face-on molecular orientation, the OBHJ-45 film with smallest diameter of P3HT nanoapillar arrays gives larger interfacial areas, higher conducting ability, efficient excitons diffusion and dissociation. The PSCs based on OBHJ-45 film exhibit significantly improved device performance, especially for the J_{sc} and FF. The SART-NIL is a powerful tool for fabricating ideal active layer for high performance PSCs at room temperature. This paper provides new insight and guidance for understanding the structure-property relationships of organic semi-conducting materials.

Acknowledgements

This work was financially supported by the National Natural Science Foundation of China (Nos. 91027040, 51473112, 21204057 and 21204058), the National Basic Research Program of China (No. 2012CB821500), the Natural Science Foundation of Jiangsu Province of China (No. BK2012213), and a Project Funded by the Priority Academic Program Development of Jiangsu Higher Education Institutions (PAPD), and the BL14B1 Beam Line at the Shanghai Synchrotron Radiation Facility in China.

Notes and references

1. G. Yu, J. Gao, J. C. Hummelen, F. Wudl and A. J. Heeger, *Science*, 1995, **270**, 1789-1791.
2. G. Li, R. Zhu and Y. Yang, *Nat Photon*, 2012, **6**, 153-161.
3. R. A. J. Janssen and J. Nelson, *Advanced Materials*, 2013, **25**, 1847-1858.
4. L. Mao, Q. Chen, Y. Li, Y. Li, J. Cai, W. Su, S. Bai, Y. Jin, C.-Q. Ma, Z. Cui and L. Chen, *Nano Energy*, 2014, **10**, 259-267.
5. Y. Li, L. Mao, Y. Gao, P. Zhang, C. Li, C. Ma, Y. Tu, Z. Cui and L. Chen, *Solar Energy Materials and Solar Cells*, 2013, **113**, 85-89.
6. J. You, L. Dou, K. Yoshimura, T. Kato, K. Ohya, T. Moriarty, K. Emery, C.-C. Chen, J. Gao, G. Li and Y. Yang, *Nat Commun*, 2013, **4**, 1446.
7. Y. Yang, W. Chen, L. Dou, W.-H. Chang, H.-S. Duan, B. Bob, G. Li and Y. Yang, *Nat Photon*, 2015, **9**, 190-198.
8. H. Zhou, Y. Zhang, C.-K. Mai, S. D. Collins, G. C. Bazan, T.-Q. Nguyen and A. J. Heeger, *Advanced Materials*, 2015, **27**, 1767-1773.
9. T. Kirchartz, K. Taretto and U. Rau, *The Journal of Physical Chemistry C*, 2009, **113**, 17958-17966.
10. S. M. Lindner, S. Hüttner, A. Chiche, M. Thelakkat and G. Krausch, *Angewandte Chemie International Edition*, 2006, **45**, 3364-3368.
11. F. Yang, M. Shtein and S. R. Forrest, *Nature Materials*, 2005, **4**, 37-41.
12. R. Otero, D. Écija, G. Fernández, J. M. Gallego, L. Sánchez, N. Martín and R. Miranda, *NANO LETTERS*, 2007, **7**, 2602-2607.
13. Y. Yang, K. Mielczarek, M. Aryal, A. Zakhidov and W. Hu, *ACS Nano*, 2012, **6**, 2877-2892.
14. G. Gustafsson, O. Inganäs and S. Stafström, *Solid State Communications*, 1990, **76**, 203-208.
15. H. Sirringhaus, P. J. Brown, R. H. Friend, M. M. Nielsen, K. Bechgaard, B. M. W. Langeveld-Voss, A. J. H. Spiering, R. A. J. Janssen, E. W. Meijer, P. Herwig and D. M. de Leeuw, *Nature*, 1999, **401**, 685-688.
16. Z. Zheng, K.-H. Yim, M. S. M. Saifullah, M. E. Welland, R. H. Friend, J.-S. Kim and W. T. S. Huck, *Nano letters*, 2007, **7**, 987-992.
17. H. Sirringhaus, R. J. Wilson, R. H. Friend, M. Inbasekaran, W. Wu, E. P. Woo, M. Grell and D. D. C. Bradley, *Appl Phys Lett*, 2000, **77**, 406-408.
18. G. Li, V. Shrotriya, J. Huang, Y. Yao, T. Moriarty, K. Emery and Y. Yang, *Nature Materials*, 2005, **4**, 864-868.
19. Z. Hu, J. Zhang and Y. Zhu, *Appl Phys Lett*, 2013, **103**, 043307.
20. J. Guo, Y. Liang, J. Szarko, B. Lee, H. J. Son, B. S. Rolczynski, L. Yu and L. X. Chen, *The Journal of Physical Chemistry B*, 2009, **114**, 742-748.
21. E. D. Gomez, K. P. Barteau, H. Wang, M. F. Toney and Y.-L. Loo, *Chemical Communications*, 2011, **47**, 436-438.
22. L. J. Guo, *Advanced Materials*, 2007, **19**, 495-513.
23. S. Y. Chou, P. R. Krauss and P. J. Renstrom, *Science*, 1996, **272**, 85-87.
24. Z. Hu, B. Muls, L. Gence, D. A. Serban, J. Hofkens, S. Melinte, B. Nysten, S. Demoustier-Champagne and A. M. Jonas, *Nano letters*, 2007, **7**, 3639-3644.
25. H. Hlaing, X. Lu, T. Hofmann, K. G. Yager, C. T. Black and B. M. Ocko, *ACS Nano*, 2011, **5**, 7532-7538.
26. Z. Hu and A. M. Jonas, *Soft Matter*, 2010, **6**, 21-28.
27. M. Aryal, K. Trivedi and W. Hu, *ACS Nano*, 2009, **3**, 3077-3090.
28. N. E. Voicu, S. Ludwigs, E. J. W. Crossland, P. Andrew and U. Steiner, *Advanced Materials*, 2007, **19**, 757-761.
29. X. He, F. Gao, G. Tu, D. Hasko, S. Hüttner, U. Steiner, N. C. Greenham, R. H. Friend and W. T. S. Huck, *NANO LETTERS*, 2010, **10**, 1302-1307.
30. G. Ding, Y. Wu, Y. Weng, W. Zhang and Z. Hu, *Macromolecules*, 2013, **46**, 8638-8643.
31. A. Pallandre, K. Glinel, A. M. Jonas and B. Nysten, *NANO LETTERS*, 2004, **4**, 365-371.
32. D. Chen, W. Zhao and T. P. Russell, *ACS Nano*, 2012, **6**, 1479-1485.
33. D. Chirvase, J. Parisi, J. C. Hummelen and V. Dyakonov, *Nanotechnology*, 2004, **15**, 1317.

34. C. Li, Y. Chen, Y. Zhao, H. Wang, W. Zhang, Y. Li, X. Yang, C. Ma, L. Chen, X. Zhu and Y. Tu, *Nanoscale*, 2013, **5**, 9536-9540.
35. P. Zhang, C. Li, Y. Li, X. Yang, L. Chen, B. Xu, W. Tian and Y. Tu, *Chemical Communications*, 2013, **49**, 4917-4919.
36. J. H. Lee, D. W. Kim, H. Jang, J. K. Choi, J. Geng, J. W. Jung, S. C. Yoon and H.-T. Jung, *Small*, 2009, **5**, 2139-2143.
37. D.-H. Ko, J. R. Tumbleston, L. Zhang, S. Williams, J. M. DeSimone, R. Lopez and E. T. Samulski, *Nano Letters*, 2009, **9**, 2742-2746.
38. S.-I. Na, S.-S. Kim, J. Jo, S.-H. Oh, J. Kim and D.-Y. Kim, *Advanced Functional Materials*, 2008, **18**, 3956-3963.
39. C. F. Shih, K. T. Hung, J. W. Wu, C. Y. Hsiao and W. M. Li, *Appl Phys Lett*, 2009, **94**, 143505.
40. J. S. Kim, Y. Park, D. Y. Lee, J. H. Lee, J. H. Park, J. K. Kim and K. Cho, *Advanced Functional Materials*, 2010, **20**, 540-545.
41. A. W. Hains, Z. Liang, M. A. Woodhouse and B. A. Gregg, *Chemical Reviews*, 2010, **110**, 6689-6735.
42. H. Xin, G. Ren, F. S. Kim and S. A. Jenekhe, *Chemistry of Materials*, 2008, **20**, 6199-6207.
43. P. Ravirajan, S. A. Haque, J. R. Durrant, D. D. C. Bradley and J. Nelson, *Advanced Functional Materials*, 2005, **15**, 609-618.